One pot synthesis of Au embedded ZnO nanorods composite heterostructures with excellent photocatalytic properties

Project work submitted to the Central University of Punjab

For the award of

Master of Science

In

Chemistry

By

Rathindranath Biswas

16mscchm01

Supervisor

Dr. Krishna Kanta Haldar

Department of chemical Sciences

School of Basic & Applied Sciences

Central University of Punjab, Bathinda, Punjab-151001

May 2018

DECLARATION

I declare that the thesis entitled "**One pot synthesis of Au embedded ZnO nanorods composite heterostructures with excellent photocatalytic properties**" has been prepared by me under the guidance of **Dr. Krishna Kanta Kaldar**, Assistant Professor, Department of Chemical Sciences, School of Basic & Applied Sciences, Central University of Punjab. No part of this thesis has formed the basis for the award of any degree or fellowship previously.

Rathindranath Biswas

Department of Chemical Sciences

School of Basic & Applied Sciences

Central University of Punjab, Bathinda

Punjab-151001

Date:

CERTIFICATE

I certify that Rathindranath Biswas has prepared his thesis entitled "**One pot synthesis of Au embedded ZnO nanorods composite heterostructures with excellent photocatalytic properties**", for the award of M.Sc. degree of the Central University of Punjab, under my guidance. He has carried out this work at the Department of Chemical Sciences, School of Basic & Applied Sciences, Central University of Punjab.

Dr. Krishna Kanta Haldar

Assistant Professor

Department of Chemical Sciences

School of Basic & Applied Sciences

Central University of Punjab

Bathinda-151001

Date:

ABSTRACT

One pot synthesis of Au embedded ZnO nanorods composite heterostructures with excellent photocatalytic properties

Name of student: Rathindranath Biswas

Registration number: 16mscchm01

Degree for which submitted: M.Sc. Chemical Science

Name of supervisor: Krishna Kanta Haldar

Name of centre: Department of Chemical Sciences

Name of school: School of Basic & Applied Sciences

Key words: Nanorods, Composite, Photocatalyst, plasmon absorption, Photodegradation.

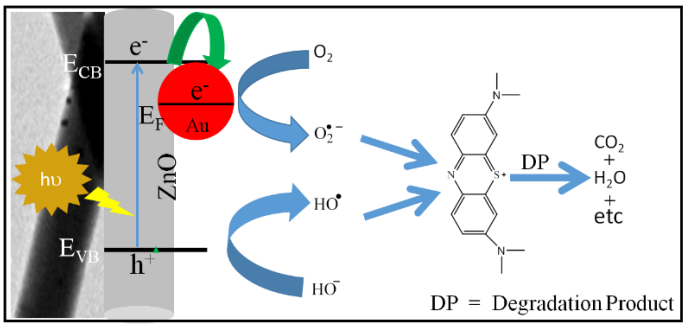

Abstract: Here, we have designed a noble composite nanostructure by embedding Au nanoparticles into ZnO nanorods surface in one pot synthesis as a photocatalyst. The formation the composite nanostructure was confirmed by X-ray diffraction, X-ray photoelectron spectroscopy (XPS), field emission scanning electron microscopy (FESEM) and transmission electron microscopy (TEM) investigations. Microscopic studies suggest that spherical Au nanoparticles are nucleated on the ZnO nanorods surface. XPS shows shifting of peak positions towards higher binding energy indicating charge transfer from ZnO to Au in the composite nanostructures. This is unambiguously confirmed by the steady state spectroscopic studies. It is found that 95.7% of Methylene blue (MB) dye is degraded by the composite nanostructure after 140 min under UV light illumination, and the apparent rate constant is found to be 0.013 min^{-1}. This new class of Au nanoparticles embedded ZnO nanorods composite nanostructure opens up new possibilities in photocatalytic, solar energy conversion, photovoltaic, and other new emerging applications.

Rathindranath Biswas **Dr. Krishna Kanta Haldar**

Dedicated to my beloved family

ACKNOWLEDGEMENT

This project is the end of my journey in obtaining my M.Sc. I have not travelled in a vacuum in this journey. This project has been kept on track and been seen through to completion with the support and encouragement of numerous people including my well-wishers, my friends, and colleagues. Also, I would like to thank all those people who made this project possible and an unforgettable experience for me. At the end of my project, it is a pleasant task to express my thanks to all those who contributed in many ways to the success of this study and made it an unforgettable experience for me.

I would like to pay my sincere thanks to honorable Vice Chancellor **Prof. R.K. Kohli** for providing me the entire infrastructure for my research work.

I am extremely indebted to our Dean Academic affairs **Prof. P. Ramarao** and H.O.D **Dr. Rajesh Kumar**, Associate Professor, Department of Chemical Sciences, School of Basic and Applied Sciences, for providing necessary infrastructure and resources to accomplish my research work for his valuable advice, constructive criticism and his extensive discussions around my work.

At this moment of accomplishment, first of all, I pay honor to my supervisor **Dr. Krishna Kanta Haldar**, Assistant Professor, Department of Chemical Sciences, School of Basic and Applied Sciences. This work would not have been possible without his guidance, support and encouragement. Under his guidance, I successfully overcome my difficulties and learned a lot. I can't forget his hard times. Despite of his busy schedule, he used to review my project progress, give his valuable suggestions and made corrections. His unflinching courage and conviction will always inspire me, and I hope to continue to work with his noble thoughts. I am very much thankful to him for picking me up as a student at the critical stage of my M.Sc. I can only say a proper thanks to him through my future work.

I would like to thank **Dr. Rajendra Singh Dhayal,** Assistant Professor, **Dr. J.N. Babu**, Assistant Professor, **Dr. Rakesh Kumar**, Assistant Professor, Department of Chemical Sciences, **Dr.Biplab Chatterjee**, Assistant Professor, Department of Chemical Sciences for their help and support .

I expand my thanks to **Mr. Dushyantha Reddy**, **Mr. Preeti Prabhat and Mr. Radhakrishan Sadh** and Lab Assistant, Department of Chemical Sciences, **Mr. Rajesh Tiwari**, Junior Technical Lab Assistant, Department Pharmaceutical sciences and natural products, Staffs of Computer lab and Staffs of Library.

I am indebted to many student colleagues for providing a stimulating and fun-filled environment. My thanks go in particular to **Ms. Samreet khirid, Ms. Pavneet**, **Ms.sangeeta Meena** and **Ms. Mansi Garg** Research Scholar, Department of Chemical Sciences, with whom I started this work and many rounds of discussion with her helped me a lot. I am ever indebted to my group mates for **Rakesh** and **Imtiaz** their distinguished helping nature with valuable support and encouragement. I wish to thanks my best friends **Sandeep, Ram singh, Sambit** ,**Swayam, Rohtash, Nikhil, Mange, Bhupender, Harshita, Manoj, Vishal, Jitender** and **Sonali,** for their love, care, and moral support. Words are short to express my deep sense of gratitude towards **Mr. Rabindra Kumar**, Scientific Officer, Central University of Punjab.

Last but not the least, I would like to pay high regards to my parents (Rakshakar Biswas and Basumati Biswas), uncle, brother and sister, for their sincere encouragement and inspirational throughout for my research work and lifting me uphill this phase of life. I owe everything to them. Besides this, several people have knowingly and unknowingly helped me in the successful completion of this dissertation, and I would like to thank everybody who was important to the successful realization of the project, as well as expressing my apology that I could not mention personally one by one.

TABLE OF CONTENT

LIST OF FIGURES

LIST OF ABBREVATIONS

Sr. No.	Full Form	Abbreviation
1	Nanoparticles	NPs
2	Nanorods	NRs
3	Nanowires	NWs
4	Ultraviolet-Visible	UV-Vis
5	Scanning Electron Microscope	SEM
6	Transmission Electron Microscope	TEM
7	High Resolution Transmission Electron Microscope	HRTEM
8	X-ray Diffraction	XRD
9	X-ray Photoelectron Spectroscopy	XPS
10	Photoluminescence	PL
11	electrochemical impedance spectroscopy	EIS
12	tri-sodium citrate	TSC
13	Methylene Blue	MB
14	energy dispersive spectroscopy	EDS
15	selected-area electron diffraction	SEAD
16	tetraoctylammonium bromide	TOAB
17	stearic acid	SA
18	1-octadecene	ODE
19	trioctylphosphine	TOP
20	poly vinyl pyrrolidone	PVP

Chapter- 1

Introduction

Chapter- 1

Introduction

Nanomaterial:

Material with any dimension between 1 to 100 nm is called as nanomaterial. There are four types of nanomaterials, they are 0 dimensional (0D), 1 D, 2 D and 3 D nanomaterial.

a) Zero dimensional nanomaterial (0D): All of the three dimensions of the material are in the range of 1 to 100 nm. For example: Quantum dots. Fullerene, Core/shell materials etc.

b) One dimensional nanomaterial (1D): Two dimensions are in 1 to 100 nm range and the other dimension is beyond 100 nm. Examples are nanorods, nanowires, nanotubes, nanofibers etc.

c) Two dimensional nanomaterial (2D): One dimension is in the range of 1 to 100nm and the other two dimensions are beyond 100 nm. For example: nanoplates, nanosheet, nanobelts, nanofilms etc.

d) Three dimensional nanomaterials (3D): Three-dimensional nanoparticles with the length of few nanometers in all three coordinate directions. Tetrapod-shaped hetero-nanostructure(Haldar et al. 2017) flower-shaped hetero-nanostructures, core/shell-shaped nanoparticles are best examples of three-dimensional nanoparticles.

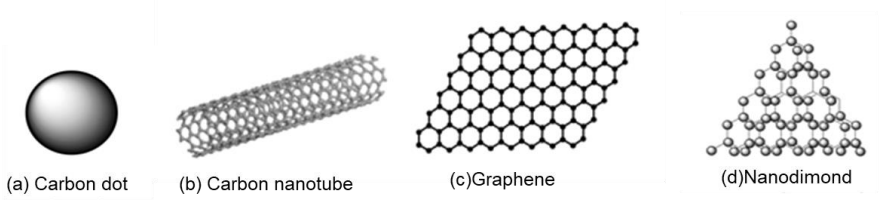

Figure 1.1 Classification of Nanomaterials:
(a) 0D, (b) 1D, (c) 2D (d) 3D Nanomaterials

:

Why Nanomaterials are so special:

As particle size decreases surface to volume ratio increase. Nanomaterials possess far larger surface areas than similar masses of larger-scale materials. As surface area per mass of a material increases, a greater amount of the material can come into contact with surrounding materials, thus the reactivity of nanomaterials change from the bulk materials. The physical properties such as melting point, boiling point, fluorescence, electrical conductivity, colour, solubility, heat capacity, magnetic permeability, and chemical reactivity change as a function of the particle size.

Quantum Effect:

In bulk material, of micron size, the electrons of the constituent atoms can move freely inside the material. When size is reduced to nanometer range, the electrons are confined to a small space, which causes quantization in their allowed energy states. In bulk material the mean free path or de-Broglie wave length of electron is much smaller than the sample dimensions. When any one, two or all three dimensions of material become comparable to the mean free path of carriers, quantum size effects not only become apparent and but also dominate the electronic and optical properties of the materials.

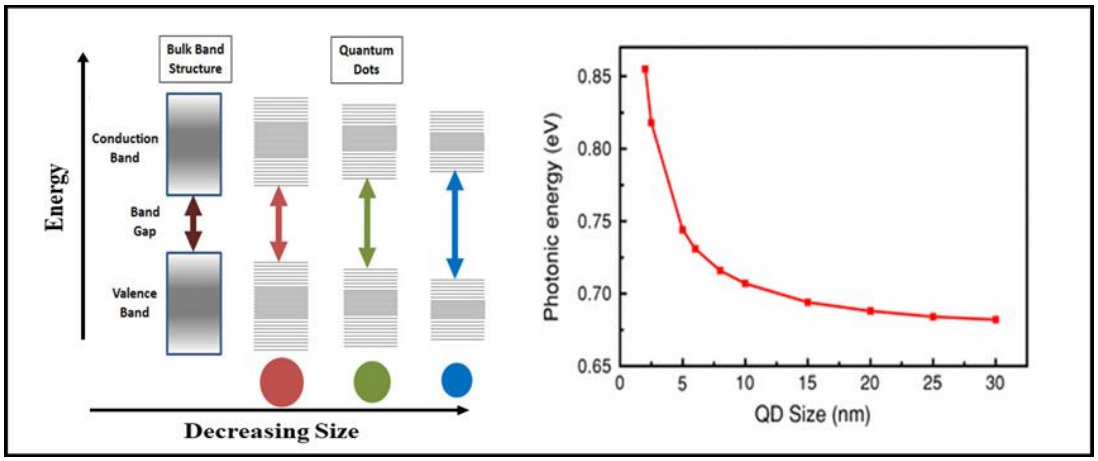

Figure 1.2 Quantum confinement effect

A fascinating and powerful result of the quantum effects of the nanoscale is the concept of “tunability” of properties. That is, by changing the size of the particle, a scientist can literally fine-tune a material property of interest (e.g., changing fluorescence colour; in turn, the fluorescence colour of a particle can be used to identify the particle, and various materials can be “labeled” with fluorescent markers for various purposes). Another potent quantum effect of the nanoscale is known as “tunneling,” which is a phenomenon that enables the scanning tunneling microscope and flash memory for computing.

Chapter- 2

Review of literature

Chapter- 2

Review of literature:

2.1. Two Different Approaches to Nanofabrication:

a) Top-down: As the name suggests, the top-down approach means from top (larger) to bottom (smaller). This approach is similar to making a statue made of stone. As in making of a statue, a bulk or big piece of stone is taken, similarly in top-down approach; a bulk piece of material is taken. Then carving and cutting is done until desired shape is achieved. Example: Different kinds of lithographic techniques cutting (such as electron beam, photo ion beam or X-ray lithograph cutting), etching, grinding, ball milling.

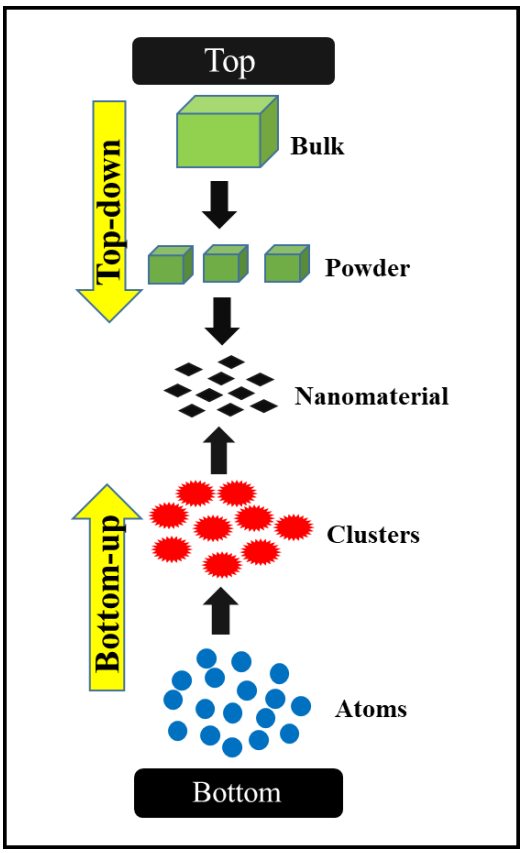

Figure 2.1 Schematic representation of Top-down and Bottom-up approach

b) Bottom-up: As the name suggests, the bottom-up approach means from bottom (smaller) to top or up (larger). In this approach we synthesis the nanomaterials by self-assembling the atoms or molecules, according to a natural physical principle or an externally applied driving force. Examples: self-assembling in chemical route synthesis of nanomaterials.

2.2. Synthesis of Nanomaterials by Chemical Methods:

Advantages of chemical synthesis:

- This is an easy techniques.
- Cheap and less instrumentation compared to many physical methods.
- Low temperature (< 350 ^{0}C) synthesis.
- Doping of foreign atoms (ions) possible during synthesis.
- Large quantities of the material can be obtained.
- Variety of sizes and shapes are possible.
- Materials are obtained in the form of liquid but can be converted into dry powder or thin films quite easily.
- Self-assembly or pattering is possible.

There are several methods for synthesis of nanoparticles. They are discussed below.

2.2a. Sol- Gel Method: Sols are solid particles in a liquid. Gels are continuous network of particles with pores filled with liquid. Sol-gel process involves formation of sols in a liquid and then connecting the sol particles to form a network. Synthesis of sol gel in general involves hydrolysis of precursors, condensation followed by polycondensation to form particles.

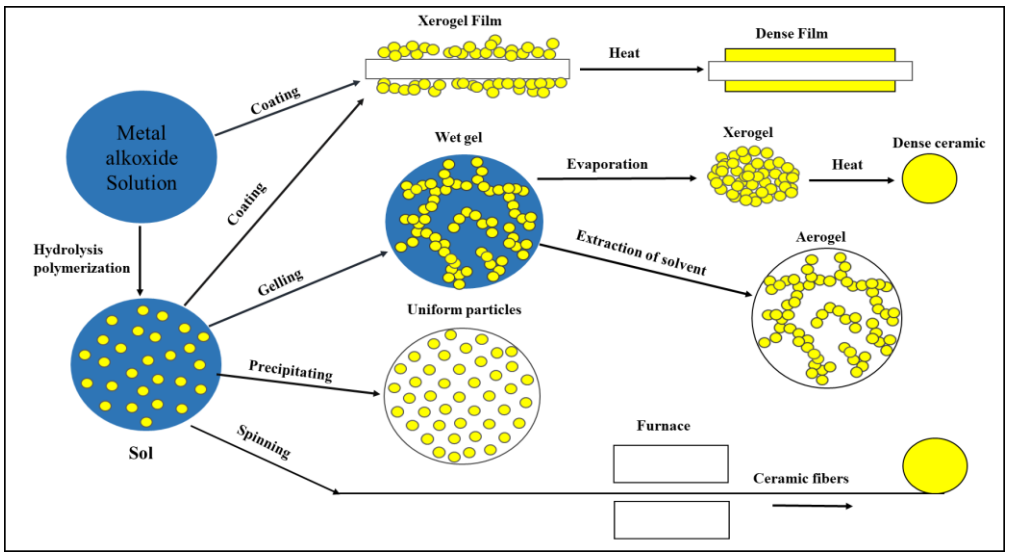

Figure 2.2 Schematic representation of Sol-Gel technologies and their products

Advantages of Sol-Gel Process:

- It is a low temperature process and this process deals with less pollution
- It produces highly pure and well controlled samples.
- It is not expensive and is also possible to synthesize nanoparticles, nanorods nanotubes etc.
- It is possible to obtain powders, thin film.
- It is particularly useful to synthesize metal oxides although sulphides, borides and nitrides are also possible.

2.2b. Solvothermal Synthesis:

Solvothermal synthesis is a method for preparing a variety of materials such as metals, semiconductors, ceramics, and polymers. The process involves the use of a solvent under moderate to high pressure (typically between 1 atm and 10,000 atm) and temperature (typically between 100 °C and 1000 °C) that facilitates the

interaction of precursors during synthesis. If water is used as the solvent, the method is called “hydrothermal synthesis.” The synthesis under hydrothermal conditions is usually performed below the supercritical temperature of water (374 °C). The process can be used to prepare many geometries including thin films, bulk powders, single crystals, and nanocrystals. In addition, the morphology (sphere (3D), rod (2D), or wire (1D)) of the crystals formed is controlled by manipulating the solvent supersaturation, chemical of interest concentration, and kinetic control. The method can be used to prepare thermodynamically stable and metastable states including novel materials that cannot be easily formed from other synthetic routes. Over the last decade, a majority (~80%) of the literature concerning solvothermal synthesis has emphasised on nanocrystals; therefore, this review will highlight some advances in nanocrystalline solvothermal synthesis.

2.2c. Sonochemical Synthesis:

In this technique the reactivity of the precursors is enhanced by taking the advantage that large amount of energy can be released when bubbles burst in a liquid. Bubbles are formed by using ultrasonic waves in a range of 20 kHz to 2 MHz. This can be considered as an alternative method to enhance the chemical reactions in liquids by heating and/or pressurizing.

2.2d. Microwave Synthesis: In a microwave apparatus heating is caused only due to a process in which molecules in a solution try to orient their dipoles appropriately to align themselves in the direction of the electric field. In the process they too oscillate, generating heat in the medium. Advantage in this case is that the external energy is not wasted during the heating of the vessel**.**

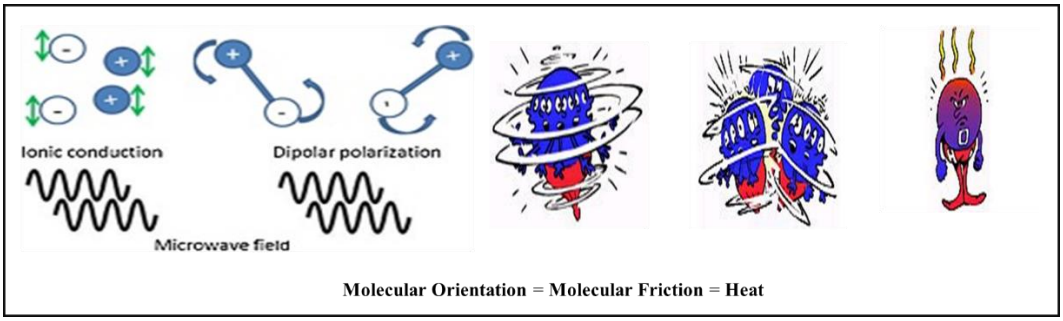

Figure 2.3 Mechanism of Microwave synthesis

2.3. Metal Nanostructures:

In recent years, the increasing number of published papers indicate great interest of engineers and scientists for the importance of metal nanoparticles (NPs) such as silver (Ag), gold (Au) and copper (Cu) etc., due to their physicochemical properties, nanometer (nm) size and surface plasmon behaviour.(Rao et al. 2002) (Stockman 2011). These metal NPs are used in catalysis, electronics for circuit enlargement and as self-assembled new nanostructure materials, but only few shows various sets of applications when they are interacted with light. Plasmonic is the interaction of light in a field with metal nanostructures(Brongersma and Shalaev 2010) (Gramotnev and Bozhevolnyi 2010) The plasmonic nanostructure materials are defined by means of their strong interaction with incident light and free electrons, where metal nanostructures play role as a source to convert light into localized electric field (electromagnetic excitations coupled with collective oscillations of free electrons) in metals(Kawata 2001), and called as localized surface plasmon. Incident light can effort more effectively with firmly controlled size and shape of metal nanostructures(Barnes et al. 2003). Nanoplasmonic research is successfully making interest because of its divers worth seeing applications, such as super lenses, surface enhanced Raman spectroscopy (SERS), single molecule spectroscopy(Jiang et al. 2003) (Kühn et al. 2006) (Nie and Emory 1997).plasmon-enhanced fluorescence, nanoscale lasing, enhancement of non-linear optical signals, quantum computing, plasmon assisted photo lithography, photocatalysis, light harvesting, biochemical sensing and possibly conversion of solar to chemical energy with plasmonic metal nanostructures(Kamat 2002). In last few years, Au and Ag nanostructures have been synthesised on a large scale for plasmonic applications. Not only for the exclusive and suitable physicochemical properties of Ag but also the price of Ag is 50 times lower than Au and that's why Ag became a good candidate in plasmonics for the next generation plasmonic technologies(Rang et al. 2008) (Wiley et al. 2007). It is to keep in mind that plasmonics restrict to a coupling between electromagnetic excitation and metal nanostructure for the generation of surface plasmon and do not show plasmonic functions in the absence

of incident light. Nanoplasmonic is quite unique as different sizes of nanostructures from 10 to 100 nm can be used which act as a link between nano and micrometer levels. Thus, plasmonics is a new subfield of nanotechnology which has ambition to understand the control of light with metal nanostructure in advanced approach.

Synthesis Of Ag nanoparticles: There are several methods for the synthesis of metal nanoparticles such as seed mediated growth process, polyol process, citrate reduction process, light mediated synthesis, self-assembly, Soft and hard template directed growth, electrolysis etc. Xinyi Dong et.al synthesised Ag nanoparticles by Stepwise Citrate Reduction i.e., Turkevich method(Dong et al. 2009). First of all 100-mL aqueous trisodium citrate (7.0 mM) was prepared in a 250-mL flask, containing controlled amounts of citric acid or NaOH at room temperature. Nitric acid or sodium hydroxide solution was added to vary the pH of various reaction solutions. The solution with different pH values (from 5.7 to 11.1) was first brought to a boil while being stirred. The reaction was started by adding 1.0 mL of 0.1 M aqueous silver nitrate. It was observed that the colour of the reaction solution change generally from colourless to yellow, then turbid. At last there was no more change in the colour of the reaction mixture which indicates the reaction was completed. The stepwise method was carried out by fast nucleation at higher pH value and the solution was suddenly adjusted to pH 6.1 by addition of HNO_3 at the end of the nucleation stage.

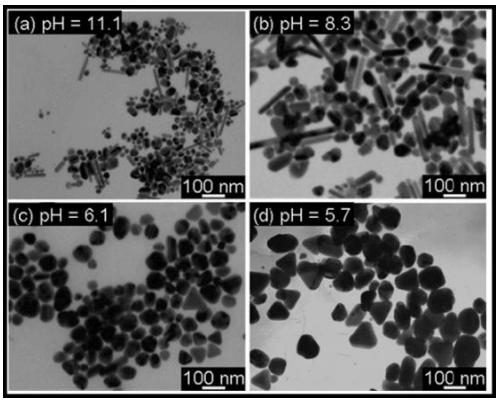

Fig 2.4 Transmission electron images for the silver nanoparticles synthesised under pH values of 11.1, 8.3, 6.1, and 5.7.

Under high pH, the product was composed of both spherical and rod shaped as a result of the fast reduction rate of the precursor. Under low pH, the product was

mainly dominated by triangle or polygon silver nanoparticles because of the slow reduction rate of the precursor.

Yugang Sun et.al followed the polyol process to synthesis silver nanowires(Sun et al. 2002). At first they synthesised Pt nanoparticles by reducing $PtCl_2$ with ethylene glycol in reflux condition at ~160 °C. In this so-called polyol process, ethylene glycol act as olvent as well as reducing agent. When $AgNO_3$ and poly vinyl pyrrolidone (PVP) were added to this refluxing solution that contained Pt seeds, silver nanoparticles were formed immediately through the reduction of $AgNO_3$ by ethylene glycol. After the $AgNO_3$ solution had been added for ~18 min, the reaction mixture turned turbid and the colour of the solution became grey. Nanowires started to appear in the reaction mixture when a small portion of the solution was taken from the vessel and viewed under an optical microscope. As the reaction mixture was refluxed at ~160 °C, it has been observed that the number and length of these nanowires increased over a period up to ~60 min. The formation of Ag nanowires was confirmed by the TEM images. The formation of Ag nanowires was also confirmed by the UV spectroscopy and XRD study. That all things are explained here in details.

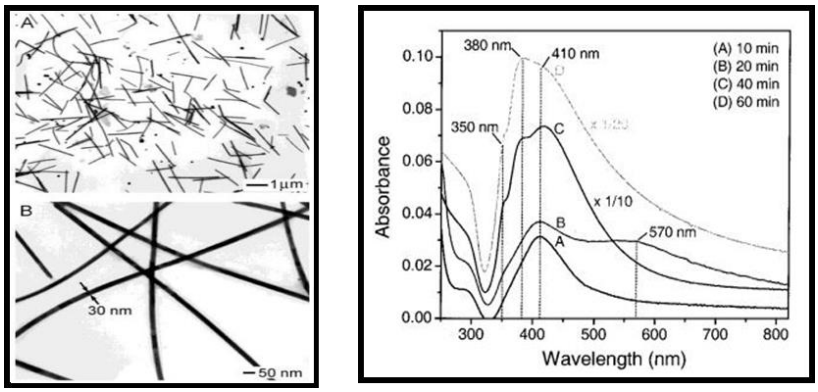

Figure 2.5a TEM images of Ag nanowires. Figure 2.5b UV-vis absorption spectra of the reaction mixture after $AgNO_3$ and PVP were added for (A) 10, (B) 20, (C) 40, and (D) 60 min.

The UV spectra was taken by diluting the solution by 30 times of water. There are four major absorption peaks at 350, 380, 410, and 570 nm. This peaks were attributed to the plasmon resonance peaks of silver with various origins: long

nanowires similar to the bulk silver, transverse mode of nanowires or nanorods, surface plasmon of nanoparticles, and the longitudinal mode of nanorods. They also measured the transport property at room temperature which designates that these nanowires were electrically continuous with a conductivity of approximately 0.8×10^5 S/cm.

Synthesis of Au NPs and NRs:

Stephan synthesised Au nanoparticles and they studied dependence the plasmon absorbance which depends on temperature as well as the size of Au nanoparticles of 9, 15, 22, 48, and 99 nm.(Link and El-Sayed 1999) The colloidal gold nanoparticles were prepared following a method introduced by Turkevich. 5 mg of Au was added to a volume of 95 mL of a chlorauric acid ($HAuCl_4$) solution which was refluxed and 5 mL of 1% sodium citrate solution was added to the boiling solution. Gold ions were reduced completely by the citrate ions after 5 min while the solution is further boiled for 30 min and then it was left to cool to room temperature. This method produced spherical particles having average diameter of about 20 nm. Although the actual value of the mean size might vary to some extant from each preparation, the size distribution was found to be always about 10% standard deviation. Larger particles were produced by the reduction of $HAuCl_4$ with hydroxylamine hydrochloride in the presence of already existing gold nanoparticles from the preparation described above. Hydroxylamine hydrochloride is a reducing agent but cannot act as a nucleating. It acts only as a growth agent in slightly acidic conditions, the particle size of the existing particles is steadily increased. The 20 nm particles therefore form the nuclei of the larger ones. Gold nanoparticles with an average diameter of about 10 nm were synthesised by reversing the order of addition of gold salt and sodium citrate. That means 68 mg of sodium citrate was added in 105 mL water are boiled and then 1 mL of aqueous solution containing 9.5 mg $HAuCl_4$ is added. The whole solution was boiled for 15 min. The plasmon bandwidth is found to follow the predicted behaviour as it increases with decreasing size in the intrinsic size region. A small temperature effect is examined. This is reliable with the fact that the dominant electronic dephasing mechanism involves electron-electroninteractions rather than electron-phonon coupling.

Gold nanorods have been prepared via electrochemical oxidation/reduction within a simple two-electrode (Yu et al. 1997). A gold metal plate (3×1×0.05 cm) is used as the anode and a platinum plate (3×1×0.05 cm) is used as the cathode in the electrochemical cell. Such an electrolytic solution was used which consist with a cationic surfactant, hexadecyltrimethylammonium bromide (C_{16}TAB, 99%; Sigma), and a rod-inducing cosurfactant. The C_{16}TAB acts as the supporting electrolyte as well as the stabilizing agent for nanoparticles to prevent their further growth. During the synthesis, the bulk gold metal were converted from the anode to form gold nanoparticles most probably at the interfacial region of the cathodic surface and within the electrolytic solution. A controlled-current electrolysis was used throughout the process for a typical current of 3 mA and a typical electrolysis time of 30 min. The synthesis was conducted under an ultrasonication and a controlled temperature, typically at 38 °C. An appropriate amount of acetone added into the electrolytic solution is necessary. The growth mechanism of Au nanorods is still not known at this stage; however, evidences advocates that the role of acetone is to facilitate the incorporation of cylindricalshaped- inducing cosurfactant into the C_{16}TAB micellar framework and inducing the cylindrical growth to form the Au-C_{16}TAB-TC_8AB system. The typical rod-inducing cosurfactant employed is an overall much more hydrophobic cationic surfactant: tetraoctylammonium bromide (C_8TAB, >98%; Fluka). Furthermore, the rod-inducing capability has also been found on several analogous surfactants, such as TC_{10}AB

2.4. Metal Oxides and hybrid nanomaterials:

Yuquan Wang synthesised VO_2 nanorods which act as Photocatalyst for Hydrogen Production (Wang et al. 2008). During the synthesis at first Si (001) wafers were supersonically washed in alcohol, acetone, and deionized water baths and placed ~ 4 cm below a sheet of vanadium (99.99%, 5 mm×50 mm×0.7 mm) connected to two copper electrodes in a vacuum chamber. The chamber was pumped to ~ 5 Pa and then a voltage of ~ 2 V was supplied to the two electrodes, as a result 65 ampere current was passing through the vanadium sheet which heats the sheet to ~ 900 °C rapidly. This helps to the deposition of nanostructures on the silicon substrate. During deposition the substrate temperature was less than 350°C. After deposition, the morphology, the structure, and the composition of the deposits were observed

by SEM, TEM, SEAD, XRD, EELS, RBS, and ultraviolet photoelectron spectrometer, respectively. The electrical and optical properties of the deposits were also measured. The photocatalytic property of the vanadium oxide nanostructures was evaluated by measuring the hydrogen evolution from a mixture of water and ethanol under UV light at room temperature.

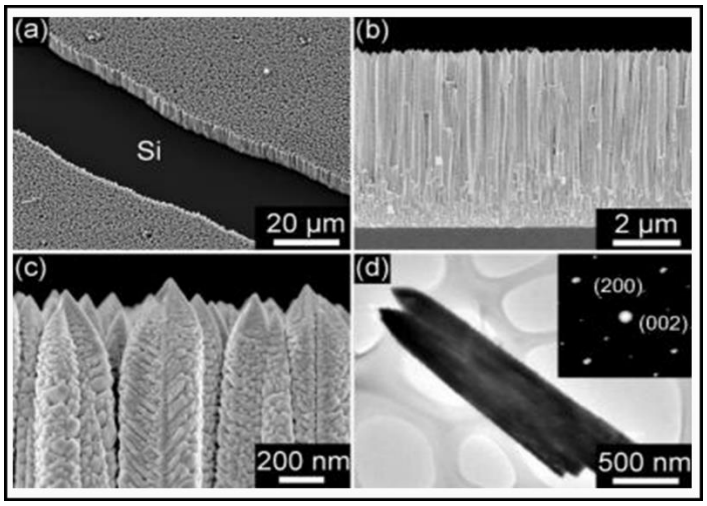

Figure 2.6 SEM images of the cone-shaped vanadium oxides rods formed on Si substrates: (a) a low-magnification image, (b) a side view image, and (c) a top-view SEM image; (d) TEM image of the rods, showing clearly the sharp tip; inset shows a corresponding SAD pattern of the rod.

The hydrogen production experiment was carried out in a quartz reactor. The reactor was cooled by running water and the entire system was hermetically sealed. The catalyst film (with a size of 5 mm×5 mm) was placed at the bottom of the quartz reactor which was filled with 20 mL of ethanol and 100 mL of water. Before the experiment nitrogen flux was introduced into the system to remove the air from the system, for 30 min. For the source of photon they used a 500 W mercury lamp which provide UV light, where the power density of UV light radiated on the catalyst film was measured to be 270 W/m^2 by a radiometer. The hydrogen evolution upon UV light radiation was measured every 20 min. Using films of the aligned VO_2 nanorods, they tuned the rate of hydrogen production by varying the incident angle of UV light on the films and reaches a high rate of 800 $mmol/m^2/h$ from a mixture of water and ethanol under UV light, at a power density of ~27 mW/cm^2.

K.K. Haldar reported a new classes of hybrid metal-semiconductor nanostructures, tetrapod hetero-structures with metal Au core and semiconductor CdSe arms

(Haldar et al. 2017). During the synthesis process, first Au nanoparticles were synthesised. 20 ml of 5 mM $HAuCl_4$ aqueous solution was mixed with 10 ml of 25 mM TOAB in toluene. After the Au precursor was transferred to the toluene layer, the toluene layer was mixed with 0.202 g dodecyl amine in 5ml toluene. Then 0.054 g $NaBH_4$ was dissolved in 3 ml H_2O and it was added drop wise to the mixture with vigorous stirring. The colour of the reaction mixture became brown which designate the formation of Au nanoparticles. To precipitate Au nanoparticles from toluene, ethanol was added and centrifuged. The Au nanoparticles were re-dispersed in 10 ml hexane. This synthesis procedure leads to the formation of Au nanoparticles which are nearly spherical shape having diameter 4 nm.

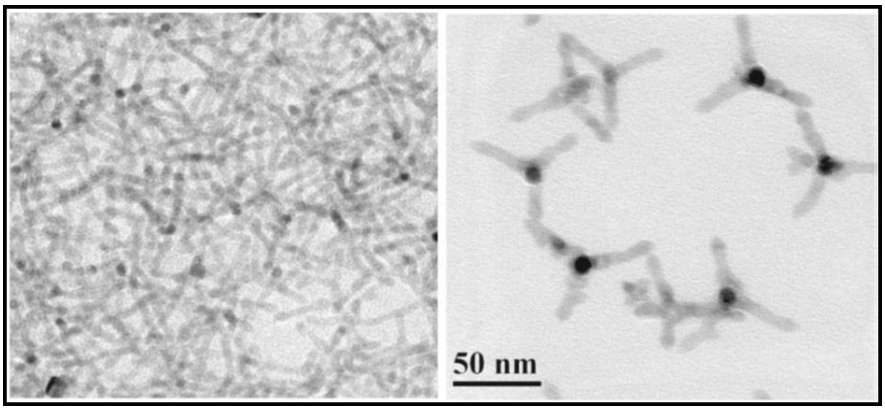

Figure 2.7 The TEM images of Au/CdSe nanotetrapod in a different view

After the synthesis of Au nanoparticles they synthesised gold-cadmium selenide tetrapod nanocrystal. Stock solution of cadmium source has been prepared using CdO (50 mg) and stearic acid (SA, 350 mg) in 10 ml 1-octadecene (ODE). The mixture was taken in a 50 ml three-necked flask then it was degassed and heated to 250 °C to get a clear solution. Then the reaction was cooled to room temperature and solution were stored in a vial. A solution of by 0.223 g selenium was dissolved in a mixture of 3 ml trioctylphosphine (TOP) and 3 ml 1-octadecene and it was heated at 50 °C temperature under stirring condition. As a result a solution of TOP-Se was prepared. Then 50 ml gold stock solution in 10 ml toluene (OD = 0.34 at 520 nm) and 10 ml ODE were taken in a separate reaction flask and degassed. After then to evaporate toluene the system was heated at 100˚C. Then the reaction temperature is increased to 280ºC. 1 ml stock solution of Se has been injected at this temperature. Just after one minute, 1.5 ml cadmium stock solution has been

quickly injected. Different time intervals samples were taken out, washed with acetone and dispersed in chloroform.

Jiahe Liang has reported the synthesis and the physical properties of chromate Nanorods/Nanobelts. During the synthesis process at first $K_2Cr_2O_7$ solution (10 mL, 0.1 M) was mixed with $Pb(Ac)_2$, $CuCl_2 \cdot 2H_2O$, $CaCl_2$, $SrCl_2$, $Zn(NO_3)_4 \cdot 6H_2O$, $Ni(Ac)_2$, $Ba(NO_3)_2$, or $AgNO_3$ solution (20 mL, 0.1 M) in a 50-mL capacity Teflon-lined stainless autoclave (Liang et al. 2005). Then it was stirred with a glass rod at room temperature. The pH of the mixture was maintained to a specific value by adding NaOH solution (1.0 M) or diluted nitric acid (1:1). The autoclave was sealed and maintained at 140 °C for 20 h and then permitted to cool naturedly. The products were filtered and washed with deionized water and absolute ethanol by three times, and it was dried at 60 °C for 6 h in air. To the adjustment of pH value of the reaction mixture they added, about 1 wt % of PVP, PEG, stearinic acid, PVA, stearylamine, CTAB, and SDS to the mixtures prior in the presence of surfactants. The reaction was carried out in a 50-mL capacity Teflon-lined stainless autoclave in a digital-type temperature-controlled oven

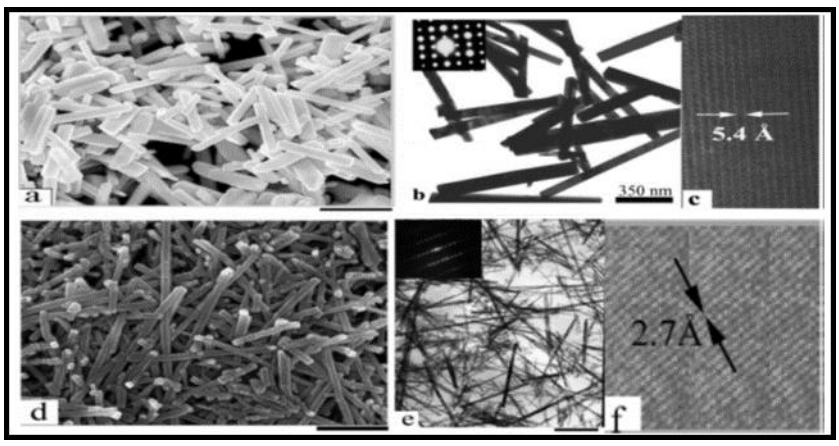

Figure 2.8 Typical electron microscopic images of $PbCrO_4$ nanorods and $CuCrO_4$ nanobelts: (a) SEM image of $PbCrO_4$ (bar = 1μm); (b) TEM image of $PbCrO_4$ (inset shows the SAED pattern); (c) HRTEM image of $PbCrO_4^{-3}$ (d) SEM image of $CuCrO_4$ (bar=0.5 μm); (e) TEM image of $CuCrO_4$ (inset shows the SAED pattern, bar=0.5 μm); (f) HRTEM image of $CuCrO_4$. To enhance the conductivity, the samples were sprayed with Au powder prior to being detected with SEM.

As a physical property they measured the electrochemical properties of the $PbCrO_4$ nanorods as electrode materials for Li-basedbatteries. During the measurement the

voltage range was fixed at 1.8-3.3 V versus Li+/Li at a constant current of ± 0.2 mA. In the first dischargeprocess, a high capacity of 163 mA h g^{-1} was found. This corresponds to the insertion of ca. 1.97 lithium/unit of $PbCrO_4$.

K.K.Haldar has synthesised NiO nanoparticles decorated ZnO nanorods composite nanostructure (Singh et al. 2018). For the fabrication of NiO nanoparticles, at first they synthesised ZnO nanorods then NiO was deposited on ZnO nanorods. ZnO nanorods were prepared by the reported methods with slight modification. Briefly, 5 7.45g zinc nitrate hexahydrate and 20g sodium hydroxide were dissolved in 50ml double distilled water. Then, 4ml of the alkali solution of zinc was mixed with 15 ml pure ethanol and 3ml ethylenediamine, followed by sonication for 30 min. Next, the solution mixture was transferred to a Teflon-lined autoclave for hydrothermal synthesis and reactions were carried out at 180°C for 24hrs in an electric hot air oven. After the reactions, the ZnO nanorods were collected by centrifugation. After then ZnO nanorods were washed repeatedly with ethanol and deionized water for NiO nanoparticles decoration. For the decoration of NiO nanoparticles, 50mg ZnO nanorods and 54 mg $Ni(NO_3)_2 \cdot 6H_2O$ were dissolved in de-ionized water (100 ml) and 0.1M sodium alginate was added to the solution to serve as stabilizing agent. NH_3 solution was added to maintain the pH below 6 so that $Ni(OH)_2$ does not form and then the whole reaction mixture was placed in a microwave oven for microwave irradiation for 30 min. Solid gel-like product was formed and it was washed by centrifugation at 6000 rpm and for further characterization it was re-dispersed in deionized water. The final products were found to be blackish in colour. They proved that the nickel oxide decorated zinc oxide composite nanorods as an excellent catalyst for photoreduction of hexavalent chromium. The fabricated environmental friendly NiO/ZnO composite nanostructure shows a well-defined photoreduction characteristic of hexavalent Chromium (Cr) (VI) to tri-valent Chromium (Cr) (III) under UV-light. This enhanced photoreduction property is credited due to the reduced electron-hole recombination process. Furthermore, it has been calculated that the photocatalytic activity rate of the NiO decorated ZnO nanorods was much higher than that of bare ZnO nanorods for the reduction of chromium (VI) and the rate is found to be 0.306 min^{-1} . These results have proved that suitable surface engineering may open up new prospects in the evolution of high-performance photocatalyst.

However, synthesis of these composite Au nanoparticles decorated ZnO nanorods materials is not straightforward like Au or ZnO nanostructures; rather, it needs a more selective approach to bring both their counterparts together. For example, the ZnO nanorods parts are synthesized at a higher temperature and Au nanoparticles were nucleated via the colloidal deposition route with polyvinyl alcohol.(Comotti et al. 2006) (Strunk et al. 2009) However, the situation remains complicated for the simultaneous nucleation and growth of the Au nanoparticles on ZnO nanorods surfaces which require a high-temperature reaction system. To best our knowledge, there is no report till date on Au nanoparticles embedded ZnO nanorods composite structure synthesized in one pot via a hydrothermal process.

Here, we have proposed to fabricate Au nanoparticles embedded ZnO nanorods composite nanostructures following the hydrothermal process and citrate reduction methods, simultaneously. These Au nanoparticles embedded ZnO composite nanostructures then manifest excellent UV-visible light directed photocatalytic performance for the photodegradation of an organic molecule such as MB in aqueous solution. Such metal-semiconductor hybrid nanostructures should have great potentials for photocatalytic properties, nonlinear optical properties, photovoltaic devices, and chemical sensors.

Chapter- 3

Material & Methods

Chapter- 3

Material & Methods

3.1. Experimental Section:

Materials: Chloroauric acid (SDFCL), zinc chlorides (Loba Chemie), trisodium citrate (Loba Chemie), methylene blue (Merck India), hydrazine (Loba Chemie), ethylenediamine (SDFCL, AR), Na_2SO_4 (Loba Chemie), acetone (AR), distilled water (18.2 millipores). The chemicals used in this work were of analytical grade and utilized without further purification. $ZnCl_2$

3.2. Preparation of Au nanoparticles embedded ZnO nanorods composite nanostructure:

Au nanoparticles embedded ZnO nanorods were synthesized in one pot via a hydrothermal process for the simultaneous nucleation and growth of the Au nanoparticles on ZnO nanorods surfaces. In a typical procedure, a 1.5g zinc chloride was dissolved in 2 ml double distilled water. Then, 2 ml of 5 M hydrazine solution was added dropwise to the zinc precursor followed by the addition of 7 ml 3.5 mM 1: 1 mixture of ethylenediamine and trisodium citrate. The whole mixture was sonication for 30 minutes. Afterward, 1 ml 25 mM chloroauric acid ($HAuCl_4$) was added to the mixture under mild stirring condition. Next, the solution mixture was transferred to a Teflon-lined autoclave for hydrothermal synthesis and reaction was conducted at 240°C for 5 hrs in an electric hot air oven. After the reactions, the Au embedded ZnO nanorods were collected by centrifugation and followed by repeated washings with acetone and deionized water and store it for characterization. We have also prepared the ZnO nanorods without Au after following the same procedure for comparing the photocatalytic efficiency of these nanorods with Au nanoparticles embedded ZnO nanorods.

3.3. Photocatalytic Studies:

The photocatalytic activity of the as-prepared Au nanoparticles embedded ZnO nanorods was tested by de-colorization of Methylene Blue (MB) dye molecule in aqueous solution at room temperature under UV light. The experiment was as

follows: aqueous solution of Au nanoparticles embedded ZnO nanorods composite (53 mg in 25 mL) was added to 50 mL of 1.8×10^{-5} mM aqueous solution of MB dye. The mixture was stirred in the dark for 30 min to attain the adsorption-desorption equilibrium. In given time intervals, analytical solution samples were taken from the suspension and immediately centrifuged at 8000 rpm for 5 min and carried absorption spectra. The quantity of MB dye in the solution was determined by measuring the absorption intensity at 663 nm, which is the main absorption peak of MB dye.

3.4. Instrumentation:

The transmission electron microscopy (TEM) images were taken using a JEOL-2100 transmission electron microscope with an operating voltage of 200kV. The scanning electron microscopy (SEM) images were taken using Carl Zeiss (Merlin compact, 2014) FESEM. The crystalline phases of the obtained ZnO nanorods and Au nanoparticles embedded ZnO nanorods composite were studied by X-ray diffraction pattern measurements which were done with Bruker Eco D8 advance X-ray powder diffractometer using Ni-filtered with Cu Kα radiation λ=1.54056 Å. The data was collected from 30˚< 2θ< 60˚ with an increment of 0.019˚. The X-ray photoelectron spectroscopy (XPS) measurements were made using Kratos Axis Ultra system, equipped with a monochromatic AlKα X-ray source. The surface was measured in as received state and after the 60s sputtering with 5 keV Ar+ ions to decrease the amount of possible contaminants from a 2x2 mm area. All measurements were performed on 0.3 mm x 0.7 mm area with 20 eV pass energy and using the charge neutralizer. Room temperature optical absorption spectra were obtained with a UV-Vis spectrophotometer (Shimadzu). The emission spectra of all samples were recorded in a FS5 steady-state fluorescence spectrometer from Edinburg instruments.

Photocurrent response was performed for Au nanoparticles embedded ZnO nanorods composite and ZnO nanorods in a photoelectrochemical system under white light irradiation. The spin-coated film of Au nanoparticles embedded ZnO nanorods composite and ZnO nanorods on Indium tin oxide coated glass (ITO) substrate was used as the photoanode in the three-electrode cell which consisted of Pt counter electrode, Ag/AgCl reference electrode, and 0.15 M Na_2SO_4 redox couple. The photocurrent transient responses were recorded by illuminating the

sample with 365nm light for 10sec and then switching off the light for another 10 sec. All measurements were carried out in ambient condition. Electrochemical impedance spectroscopy (EIS) studies were done on a Metrohm Autolab 204/ PGSTAT electrochemical workstation, and the measurements were acquired in the light at an open circuit voltage over a frequency range from 0.1 Hz to 100 kHz with an AC voltage of 50 mV.

Chapter - 4

Results and discussion

Chapter - 4

Results and discussion:

The composite of Au nanoparticles embedded ZnO nanorods were prepared by one-pot growth in the colloidal solution. It has been found that almost all the Au nanoparticles embedded ZnO composite nanorods, Au nanoparticles are attached to the ZnO nanorods surface. Figure 4.1.represents a typical SEM image of the as-prepared Au nanoparticles embedded ZnO nanorods. The SEM clearly reveals the formation of rod-like nanostructures of faceted surface planes, in which Au nanoparticles attached. Thus the formation of Au nanoparticles on the surface of ZnO nanorods is evident from the SEM images.

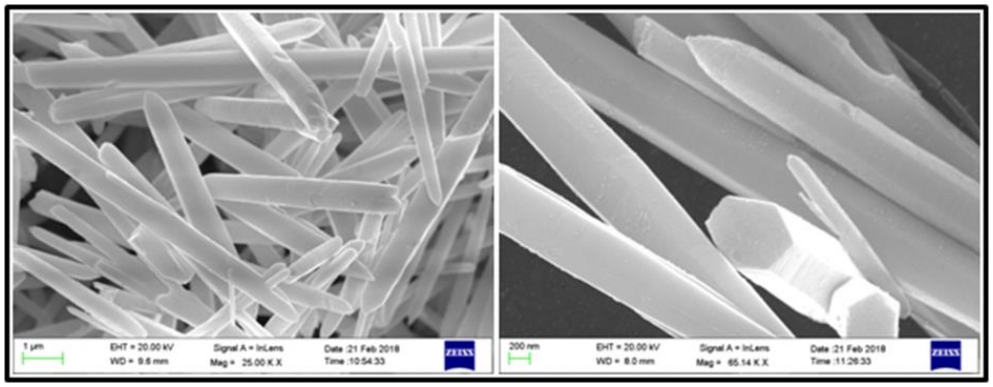

Figure4.1 Shows the SEM image of Au nanoparticles embedded ZnO nanorods prepared by one pot chemical synthesis.

Again, we have confirmed the presence of Au in the Au nanoparticles embedded ZnO nanorods composite nanostructure via TEM study. The TEM observation is continual with the SEM observation. Figure 4.2. depicts a typical bright field TEM image of the as-synthesized composite structure in which spherical Au nanoparticles are on the surface of ZnO nanorods with an average diameter of about 160-200 nm and length 3.2-3.5 μm. Figure 4.2a. reveals a wide view of the TEM images showing Au nanoparticles embedded ZnO nanorods. Without size sorting, the one-dimensional composite nanocrystals obtained here shows good monodispersity. The Au nanoparticles embedded ZnO nanorods composite structures possess a highly crystalline structure.

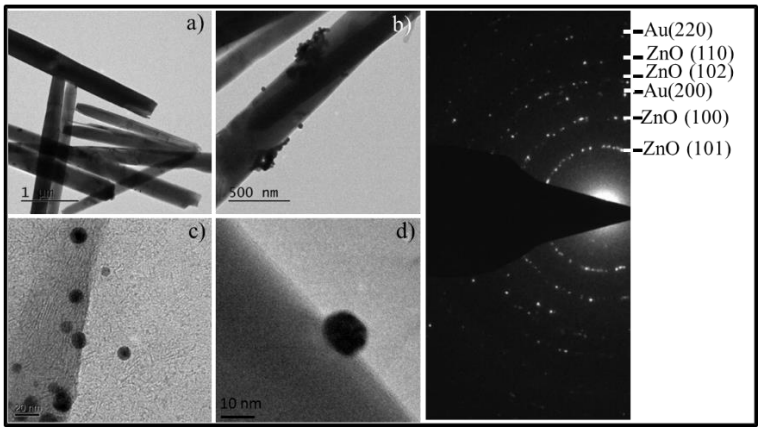

Figure 4.2 Typical TEM image of Au nanoparticles embedded ZnO nanorods in wide view (a and b) and high magnification (c and d). (e) Shows the selected-area electron diffraction (SAED) pattern for Au nanoparticles embedded ZnO nanorods composite nanostructure.

In addition, the TEM images of higher magnification (figure 4.2b. & c) affirm that the diameter of the attached Au nanoparticles about ~8-10 nm. Overall, the Au nanoparticles in all the composite structure of Au embedded ZnO nanorods are uniform in morphology. It was noticed by HRTEM images (Figure 2d) that distinct Au nanoparticles is attached to ZnO nanorod surface. Figure 4.2e. shows the selected-area electron diffraction (SAED) pattern for Au nanoparticles embedded ZnO nanorods composite nanostructure. The presence of the (101), (100), (102), and (110) planes for ZnO and (200) and (220) planes for Au again corroborates the formation of hexagonal ZnO (JCPDS card no.36-1451) and face center cubic Au (JCPDS card no.98-000-0230), respectively. Additionally, energy dispersive spectroscopy (EDS) verifies the presence of the elements Au, Zn, and O (as shown in Figure 4.3.) in the Au nanoparticles embedded ZnO nanorods.

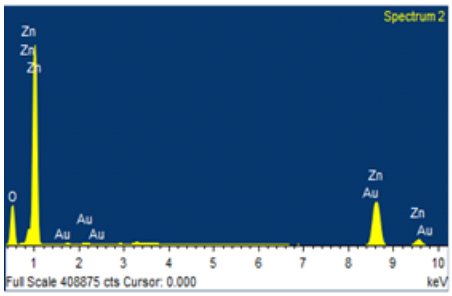

Element	Weight%	Atomic %
O K	19.85	51.42
Zn K	75.72	46.50
Au M	3.43	2.09
Total	100	

Figure 4.3 EDS Line scan mappings for elements O, Zn, and Au in the Au nanoparticles embedded ZnO composite nanorods and the table shows the composition.

Here, the ethylenediamine plays an important role in controlling the formation of rod shaped ZnO. The chelating ligands ethylenediamine present in the reaction mixture may serve as consumer to Zn^{2+} cations constraining the spiral growth of the rods and directed the growth of the ZnO nanorods.(Liu and Zeng 2003)

The Au nanoparticles embedded ZnO nanorods composite nanostructure formation process was monitored via FT-IR studies of the ZnO nanorods in presence of Au embedded samples (figure 4.4.). It is reported that the reduction of Au^{3+} to Au^{0} occurs by tri-sodium citrate present in the growth solution at boiling temperature.(Kimling et al. 2006) Thus, we believe that a similar situation would occur in the present study. The ionized sodium citrate molecules reduce Au^{3+} to Au^{0} nanoparticles in reaction medium, and it stabilizes the Au nanoparticles serving as capping agent.(Kimling et al. 2006) Next, free carboxyl group of citrate ions get bonded with the Zn atoms of ZnO nanorods by chelating through bridging between the Zn atoms and the carboxyl group of citrate along with Au and this result in attachment of Au onto the ZnO surface.(Ruiz Peralta et al. 2012)

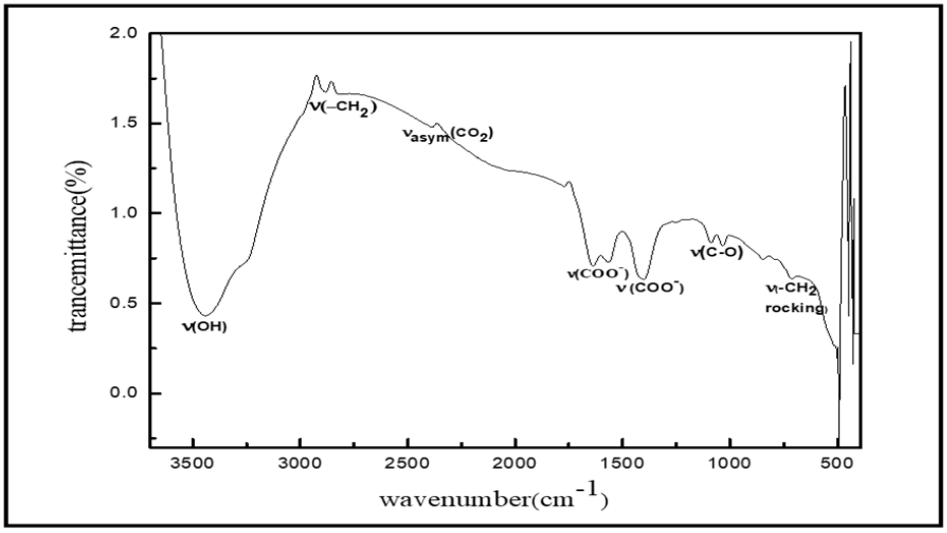

Figure 4.4 FTIR spectra of Au nanoparticles embedded ZnO composite nanorods.

The broad peak at 3300 -3500 cm^{-1} assigned the O-H stretching vibration of absorbed water molecules on the ZnO surface. Two weak peak at 2850 cm^{-1} and 2921 cm^{-1} resemble the symmetric (v_{sym}) and asymmetric (v_{asym}) stretching vibration of C-H bond of $–CH_2$ group which is present in TSC molecule, respectively. Peak at 2363 cm^{-1} is due to the O=C=O asymmetric stretching vibrational of atmospheric CO_2 molecules as the reaction was carried out in open condition. Peaks at 1402 cm^{-1} and 1560 cm^{-1} are due to the symmetric and asymmetric stretching of C=O of the carboxyl group of sodium citrate, respectively. These two peaks indicate that the carboxyl groups are in ionised form (COO^-). The peaks corresponding to 1030 and 1090 is due to the deformation of C-C bond and C-O stretching vibration mode of C-O bond, respectively. The rocking bending modes of $–CH_2$ group give a peak at 710 cm^{-1}. Bellow 700 cm^{-1}, the peaks 497 cm^{-1},493 cm^{-1},447 cm^{-1}, and 426 cm^{-1} are arised for the stretching vibration of the Zn-O bond in the ZnO lattice.

For further information regarding the crystalline structure and identify the crystal phase of Au nanoparticles embedded ZnO nanorods, we have analyzed the powder X-ray diffraction (XRD) study of ZnO nanorods in presence and absence of Au. Figure 4.5 depicts the XRD pattern of ZnO NRs and Au nanoparticles embedded ZnO nanorods. The strong peaks appear at 31.8°(100), 34.3°(002), 36.3° (101), 47.6°(102) and 56.6°(110) (figure 4.5a) clearly indicate that the as-prepared ZnO nanorods have hexagonal structure (JCPDS card no. 36-1451). On the other hand,

for the Au nanoparticles embedded ZnO nanorods, we have found one more additional peak at 38.2° (Figure 4.5b) which corresponds to (111) plane of face center cubic Au (JCPDS card no. 98-000-0230). This result demonstrates the formation of highly crystalline Au nanoparticles embedded ZnO composite nanorods. This is in good agreement with the SAED analysis (Figure 4.2e). In addition, no other crystalline impurities and no remarkable diffraction peak shifting were observed.

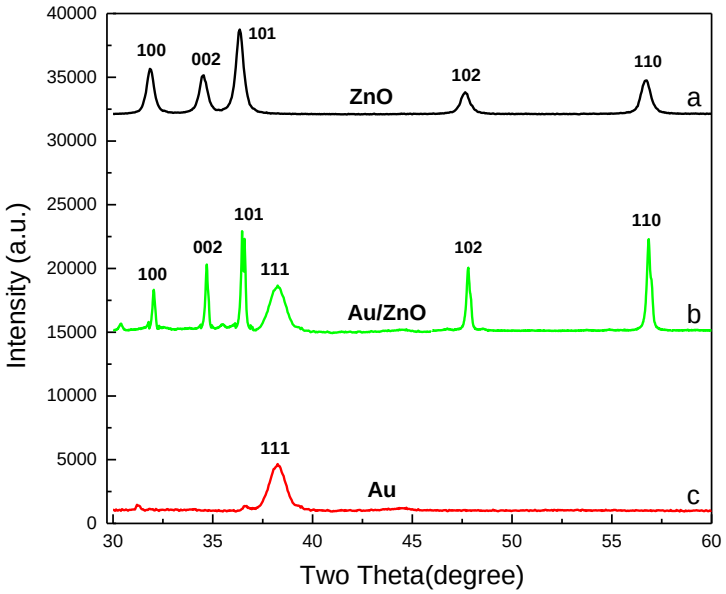

Figure 4.5 XRD pattern of (a) ZnO and (b) Au nanoparticles embedded ZnO nanorods and (c) Au nanoparticles

To further study the composition of composite nanostructures, we carried out XPS measurements. Figure 4 shows the XPS spectra of Au, Zn, and O. The energy calibration was made using the Au 4f 7/2 peak at 84.0 eV. All decompositions were made with Casa XPS using GL(m) peaks (product of m% Lorenztian and 100-m % Gaussian). The Au 4d area exhibits the 4d 5/2 and 4d 3/2 peaks at 335.4 eV and 353.5 eV (figure 4a). Only one but broad (FWHM 4.5 eV) GL(70) component is needed in the deconvolution. The relative concentration of Gold is 3.5 at-% based on the Au 3d 5/2 peak.

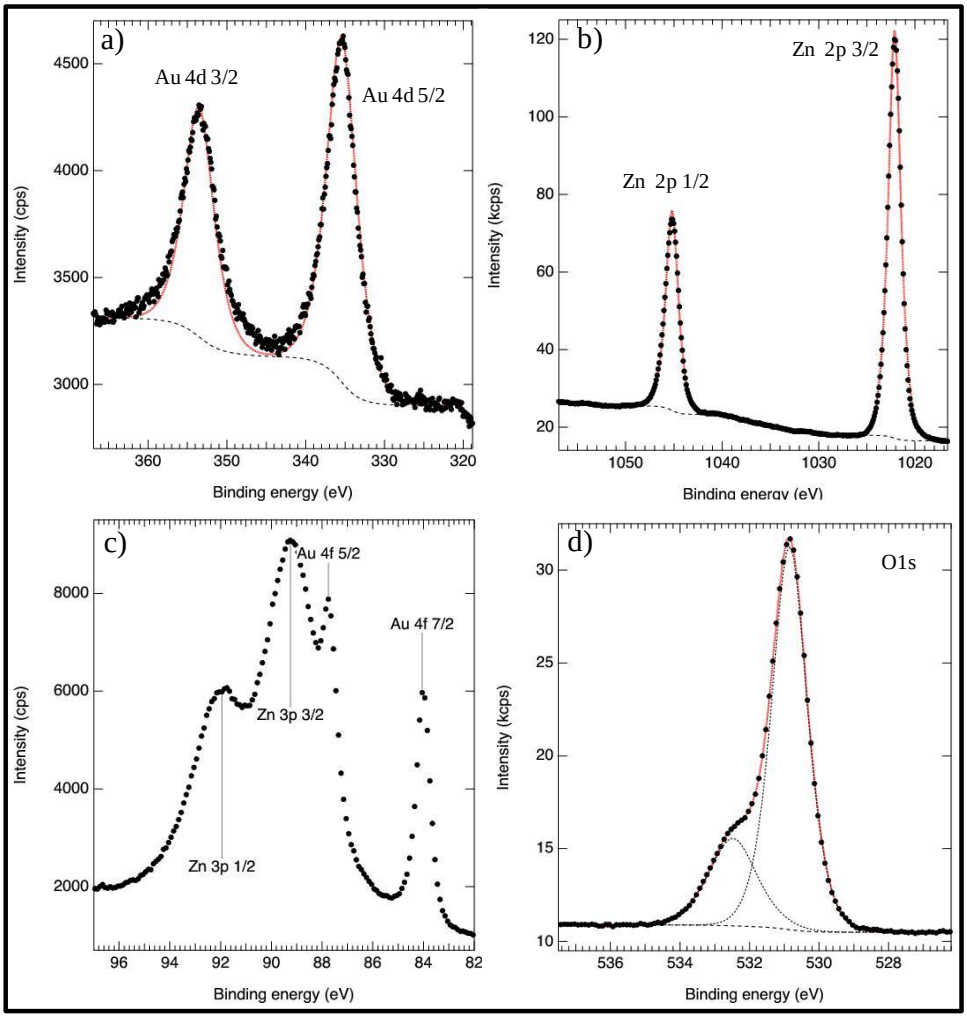

Figure 4.6 XPS spectra of (a) Au 4d and (b) Zn 2p (c) combined Au 4f and Zn 3p and (d) O 1s in Au nanoparticles embedded ZnO composite nanorods.

In the Zn 2p area the 2p3/2 and 2p1/2 peaks are visible. Both indicate only one GL(80) component (FWHM 1.5 eV) with binding energies of 1022.1 eV and 1045.2 eV (figure 4.6b). The binding energy of the 2p3/2 cannot be used to identify the chemical state since both metallic Zn (0) and Zn(II) oxide have values between 1021 eV to 1022 eV.(Bera et al. 2012) (Biesinger et al. 2010) However, the chemical state can be identified using the Auger parameter calculated using the Zn 2p3/2 peak and the LMM Auger peak. The Zn LMM Auger spectrum has a main peak at 498.5 eV and a shoulder at 495.1 eV when GL(30) peaks are used (Figure S3). The Auger parameter calculated using the main LMM peak gives a value of 2010.2 eV corresponding to Zn(II) oxide.(Biesinger et al. 2010) The relative concentration of Zinc is 39 at-% based on the 2p3/2 peak. The most intense Gold peak, Au 4f, overlap heavily with Zn 3d and we decided not to use those peaks to estimate the

concentrations. However, it is still possible to see that the Au 4f7/2 peak is narrow (FWHM 0.74 eV) and has only one component (figure 4.6c).

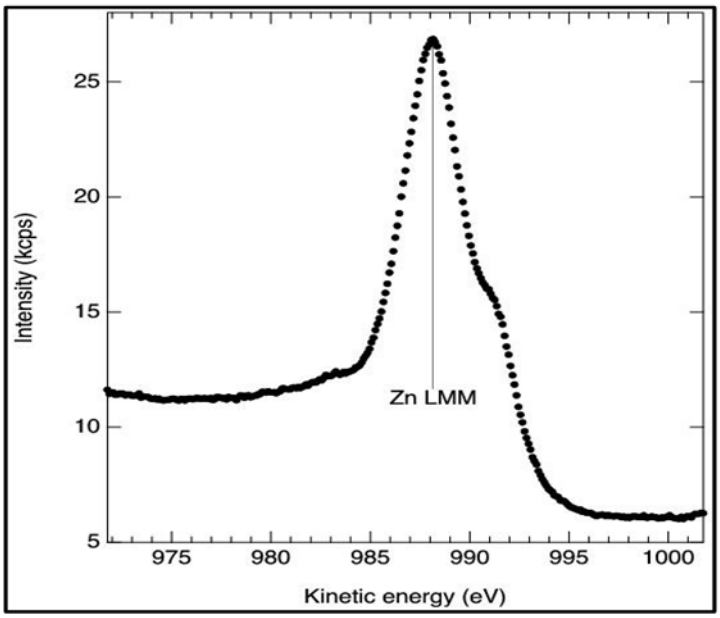

Figure 4.7 Zn LMM Auger spectrum in Au nanoparticles embedded ZnO NRs

The O1s spectrum has two components that can be assigned to oxide at 530.9 eV and hydroxide at 532.5 eV (figure 4.6d). The relative concentrations for oxide is 44 at-% and hydroxide 14 at-% based on 3deconvolution with two GL (60) peaks. Notably, compared with the pure Au nanoparticles and Au/ZnO, the binding energies of Au in such Au/ZnO composite nanorods shows a shifting of peak positions towards higher binding energy with respect pure Au nanoparticles(Klyushin et al. 2014) indicating the changes in the electronic structure due to the occurrence of charge transfer between Au nanoparticles and ZnO nanorods.(Islam et al. 1996) (Mar et al. 1993) (Yang and Fan 2002)

Figure 4.8 shows the absorption spectra of aqueous solutions of pure Au nanoparticles, pure ZnO nanorods, and Au nanoparticles embedded ZnO nanorods. The absorption spectra of both Au and ZnO change significantly upon forming directly coupled Au embedded ZnO nanorods composite structures. The plasmon bands centered at 521, and 552 nm are for pure Au and Au nanoparticles embedded ZnO nanorods, respectively. The surface plasmon band is shifted from 521 to 552 nm for Au nanoparticles embedded ZnO nanorods. The absorption peaks at 372 and 361 nm are due to excitonic band (Haldar and Sen 2016) for bare ZnO nanorods

and Au nanoparticles embedded ZnO nanorods, respectively. The blue shifting of the excitonic band (ZnO) with respect to bare ZnO nanorods (372 nm) is obviously due to the attachment of Au nanoparticles on ZnO nanorods. As reported earlier, the high dielectric constant of the TiO_2 and SnO_2 shell on Au causes a red shift in the plasmon absorption of the Au core.(Hirakawa and Kamat 2005) (Oldfield et al. 2000)

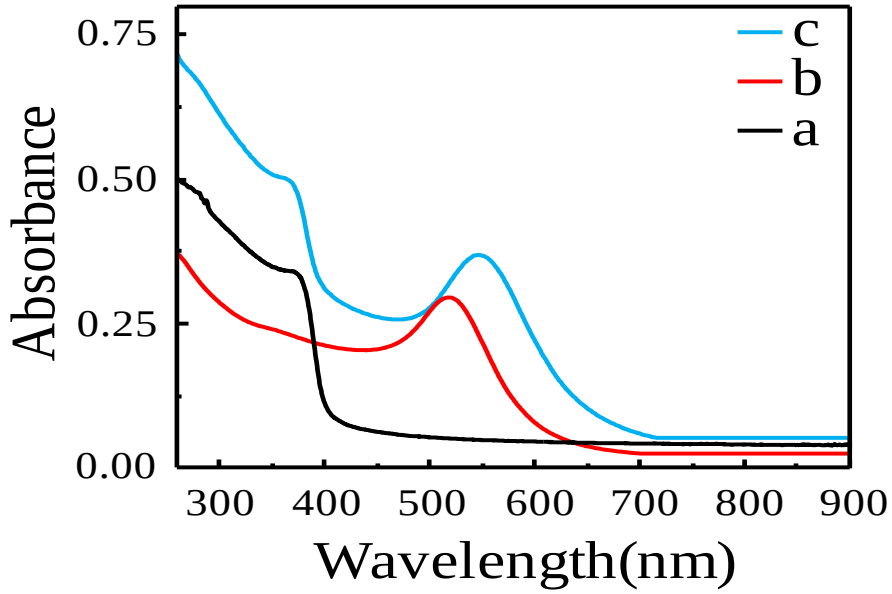

Fi gure 4.8 Absorbance spectra of (a) Pure ZnO nanorods, (b) Au nanoparticles and (c) Au nanoparticles embedded ZnO composite nanorods.

This shifting of plasmon absorption band is exploited to monitor the concentration of electrons in the Au core. It is well-known that the Fermi levels of two components equilibrate when metal nanoparticles come in contact with a charged semiconductor.(Wood et al. 2001) The Fermi level of Au is more positive (E_F = 0.4 V vs NHE) than the conduction band energy of ZnO (E_{CB} = -0.5 V vs NHE), therefore, the charge transfer from the excited ZnO to Au nanoparticles would be thermodynamically favorable.(Haldar et al. 2008) The processes that lead to storage of electrons in the Au core are summarized below.

$$ZnO + hv \longrightarrow ZnO\ (e + h)$$

$$ZnO\ (e + h) + Au \longrightarrow Au\ (e) + ZnO\ (h)$$

The photogenerated electron separation was further confirmed by comparing the photoluminescence (PL) spectra of the ZnO nanorods and Au nanoparticles embedded ZnO nanorods composite nanostructure. The characteristics of the PL spectra of the Au nanoparticles embedded ZnO nanorods composites were very analogous to bare ZnO nanorods (Figure 4.9). However, in case of Au nanoparticles embedded ZnO nanorods composites, the intensity of both the emission bands were much lower emission intensity than the corresponding bare ZnO nanorods.

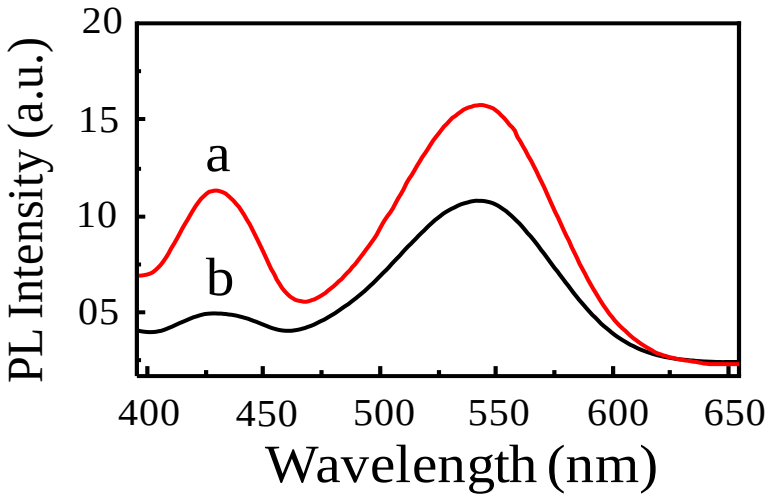

Figure 4.9. PL spectra of (a) ZnO and (b) Au nanoparticles embedded ZnO nanorods.

This PL intensity quenching arises due to the incorporation of Au nanoparticles on ZnO nanorods surface.(Lakowicz 2005) It is already reported that when metal and semiconductor has a direct connection, then electron transfer occurs from a conduction band of the semiconductor to the Fermi level of metal which are in low lying (Li et al. 2009)

To further confirm the charge transfer between Au nanoparticles and ZnO nanorods, we have measured the photocurrent response of ZnO nanorods and Au nanoparticles embedded ZnO nanorods composite counterpart electrodes by inserting them in a photoelectrochemical cell. The photocurrent responses of ZnO nanorods and Au nanoparticles embedded ZnO nanorods composite structures were shown in Figure 4.10, under illumination of light irradiation. Both of them shows quick response regarding the on/off cycle of light characteristic the electron transfer process from ZnO nanorods to Au nanoparticles.

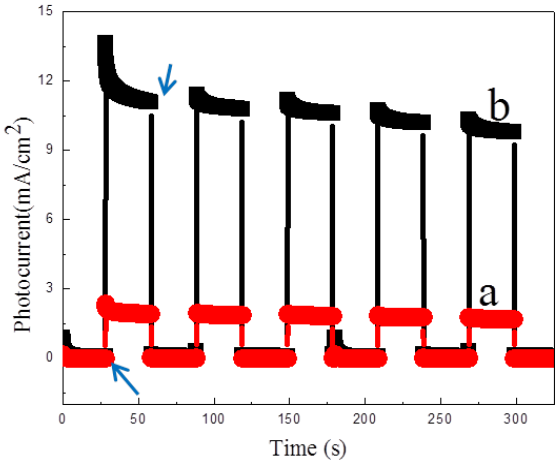

Figure 4.10. Photocurrent spectra of (a) ZnO and (b) Au nanoparticles embedded ZnO nanorods.

The result clearly demonstrates that the photocurrent response of Au nanoparticles embedded ZnO nanorods is higher compared to bare ZnO nanorods, indicating the improvement in photocurrent generation due to electron transfer from ZnO nanorods to Au nanoparticles by enhancing the lifetime of photogenerated electrons. It is believed that the electron migration mechanism from the photoexcited ZnO surface to the electron deficient Au is responsible for photocurrent generation.(She et al. 2018) (Tahir et al. 2013) Thus, the enhancement of the photoresponse speed can widen the opportunity of exploiting Au nanoparticles and ZnO nanorods composite nanostructure for superior photocatalytic activities.

For a better understanding of the origin of the commendable catalytic performance of Au nanoparticles embedded ZnO nanorods composite nanostructure, and to interpret the PL results, we explored electrochemical impedance spectroscopy (EIS) investigation. Figure 10.11 shows the electrochemical impedance spectra of the ZnO nanorods and Au nanoparticles embedded ZnO nanorods composite nanostructure, respectively. EIS result depicts that the smaller impedance semicircle radius is observed for Au nanoparticles embedded ZnO nanorods composite nanostructure with respect to bare ZnO nanorods.

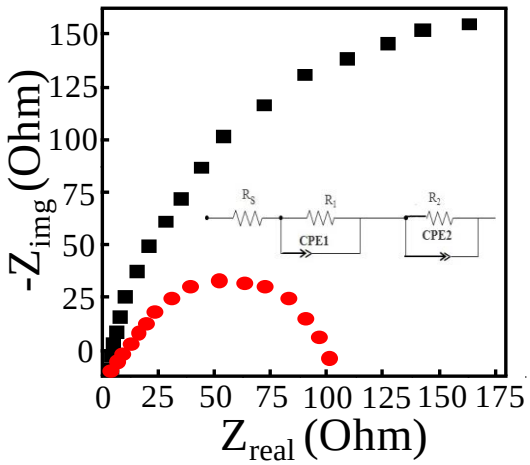

Figure 10.11. EIS spectra of (a) ZnO and (b) Au nanoparticles embedded ZnO

This result indicates that the charge recombination rate is decreased after attachment of Au nanoparticles on ZnO nanorods surface compared to bare ZnO nanorods and electron transfer ability of Au nanoparticles on ZnO nanorods composite nanostructure enhances. Thus, Au deposition on ZnO nanorods significantly hindered the recombination rate of the photoinduced charge carriers which leads to an excellent visible light directed photocatalytic application of Au nanoparticles embedded ZnO nanorods composites. This indicates the persistence of our EIS results, which also support the photoluminescence analysis. Therefore, a magnificent ability of photocatalytic activity is predictable at the surfaces of Au nanoparticles embedded ZnO nanorods composite nanostructure. A series of photocatalytic experiments were performed in this work to examine the photocatalytic properties of the as-synthesized Au nanoparticles embedded ZnO nanorods composite nanostructure.

Methylene Blue (MB), a typical dye that can be decomposed by hydroxyl radicals (Wu and Chern 2006) was used as the experiment pollutant to monitor the photocatalytic oxidation progress for Au nanoparticles embedded ZnO nanorods composite nanostructure. The time-dependent UV-visible spectra of MB solutions under UV-visible light illumination in the presence of Au nanoparticles embedded ZnO nanorods composite nanostructures were shown in Figure 4.12A. MB dye shows a major absorption band at 663 nm in aqueous solution. It is found that the absorbance of MB is gradually reduced with increased UV irradiation time for the Au

nanoparticles embedded ZnO nanorods composite nanostructure. It clearly shows that the process is slower in the case of ZnO nanorods (figure 4.12B).

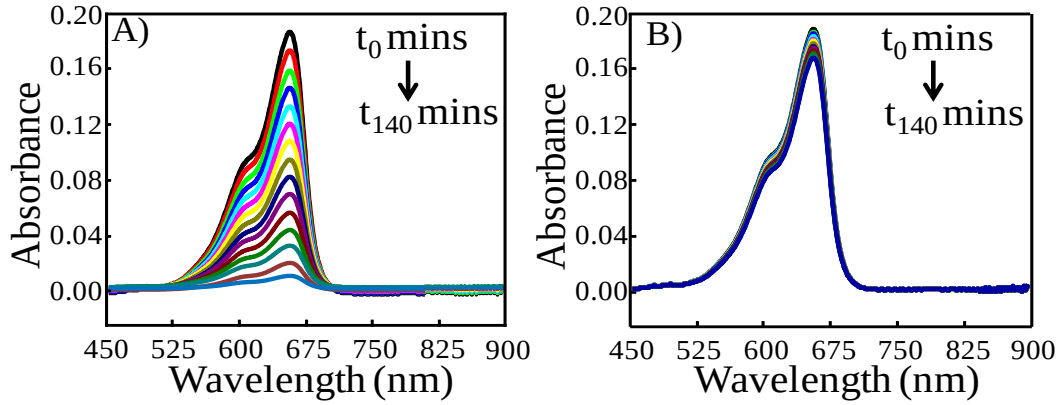

Figure 4.12. The absorbance spectral changes of MB solution in the presence (A) Au nanoparticles embedded ZnO composite nanorods and (B) ZnO nanorods.

MB-Au nanoparticles control reaction, in which tri-sodium citrate (TSC) capped Au particles of nearly 10 nm in diameter were used, is shown in the figure 4.13. ZnO nanorod and Au nanoparticles embedded ZnO nanorods composite nanostructure are tested for 140 min under identical conditions. It is found that 95.7% of MB dye is degraded by the Au nanoparticles embedded ZnO nanorods composite nanostructure after 140 min UV irradiation, whereas 10.3% degradation is observed in the case of ZnO nanorods.

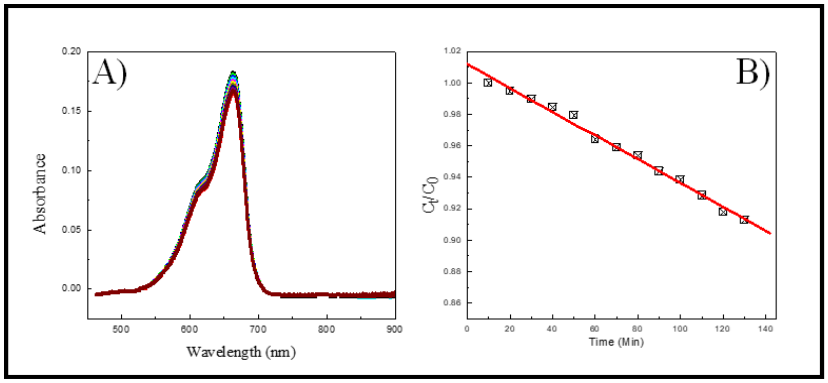

Figure 4.13 The absorbance spectral changes of MB solution in the presence of Au nanoparticles (A) and corresponding degradation of MB molecules (B).

The decomposition of MB dye under the same UV irradiation condition is negligible in the presence of Au NPs and absence of both ZnO nanorods and Au nanoparticles embedded ZnO nanorods composite nanostructure. Therefore, the large reduction of MB dye absorption in the MB/Au nanoparticles embedded ZnO nanorods composite nanostructure solution can be attributed to a photocatalytic effect that happens due to the presence of the Au nanoparticles embedded ZnO nanorods composite nanostructure. Degradation rate k_D is calculated using following equation:

$$k_D = (A_0\text{-}A)/A \qquad (1)$$

Where A_0 and A are the initial absorbance and the sample absorbance, respectively. The kinetic profiles of degradation of MB under UV light are also investigated. The photodegradation of MB follows apparently first-order kinetics. Its kinetics can be expressed as $\ln(I_0/I_t) = kt$, where k is the apparent reaction rate constant, I_0 is the concentration of MB at adsorption equilibrium, and I_t is the residual concentration of MB at different illumination time intervals. Figures 4.14A and 4.14B show the photodegradation of MB in terms of absorption spectra and as a function of irradiation time in the presence of Au nanoparticles embedded ZnO nanorods composite nanostructure and ZnO nanorods, respectively.

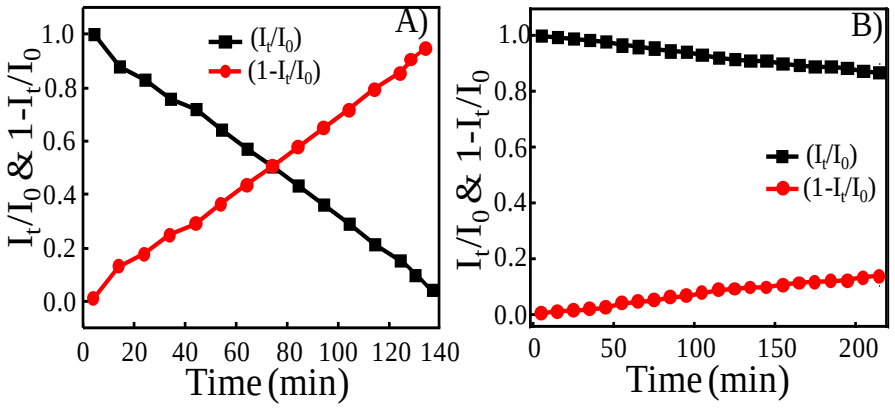

Figure 4.14 The intersection of these two curves (I_t/I_0 and $1\text{-}I_t/I_0$) shows the half-life of MB in presence of (A) Au nanoparticles embedded ZnO composite nanorods And (B) ZnO nanorods under UV light, which is the time taken for the concentration of MB to decrease by half.

The intersection of these two curves (C/C_0 and $1-C/C_0$) shows the half-life of MB, which is the time taken for the concentration of MB to decrease by half.(Soltani et al. 2012) From these figures, it could be seen that the intensity of the adsorption peaks diminished gradually as the exposure time increased, which is more pronounced in the case of using ZnO nanorods as a photocatalyst. Thereby the normalized concentration change of MB in the presence of ZnO nanorods is greater than in the presence of Au nanoparticles embedded ZnO nanorods composite nanostructure. The concentration of MB has decreased by half after 81.3 min and the degradation efficiency has reached 95.7% after 140 min while for ZnO nanorods, the efficiency was only nearly 14.7% after 140 min.

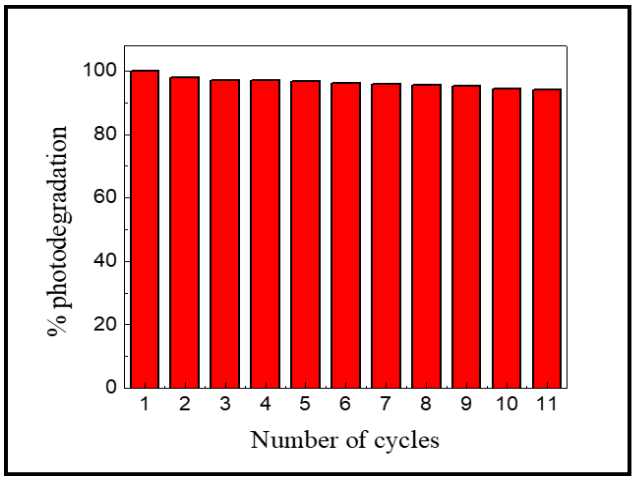

Figure 4.15 Recycling and reuse of Au nanoparticles embedded ZnO composite nanorods photocatalyst for the degradation of MB.

The lifetime of a catalyst is an important parameter for any catalytic process because of its further use for a long span of time leading to a significant cost diminution. For this reason, the Au nanoparticles embedded ZnO nanorods composite catalyst was recycled, which indicate a slowdown in efficiency only from 100% (first run) to 94.1% (11^{th} run) as shown in Figure 4.15. These results suggests that Au nanoparticles embedded ZnO nanorods composite catalyst can sustain effective and reusable under UV light. The mechanism of photocatalysis can be summarized as follows:

$$ZnO + hv \longrightarrow ZnO(e^- + h^+)$$

$$Au^0 + e^- \longrightarrow Au^-$$

$$Au^- + O_2 \longrightarrow Au^0 + O_2^-$$

$$H_2O + h^+ \longrightarrow HO^\bullet + H^+$$

$$HO^\bullet + MB \longrightarrow \text{Degradation products of MB}$$

Figure 4.16A and 4.16B show a linear relationship between (I_0/I) or $\ln(I_0/I)$ and reaction time (t), indicating that the photodegradation of MB follows a first-order kinetics model. The apparent rate constants as kinetic evidence for the samples are determined as 0.0025 and 0.016 min^{-1} for ZnO nanorods and Au nanoparticles embedded ZnO nanorods composite nanostructure, respectively.

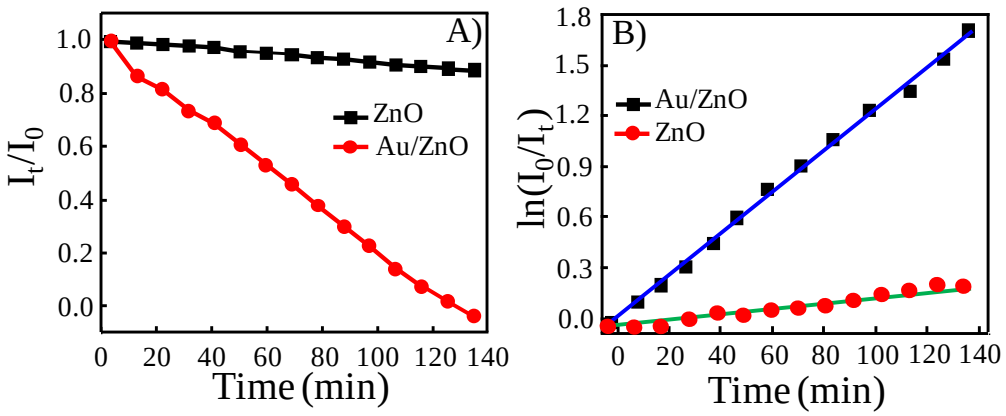

Figure 4.16 (A) Photodegradation and (B) rate of photodegradation of MB dye in presence of ZnO nanorods and Au nanoparticles embedded ZnO composite

Thus, the photocatalytic activity significantly enhances due to Au nanoparticles decoration on ZnO nanorods surface. These results clearly demonstrate that the Au nanoparticles embedded ZnO nanorods composite nanostructure has commendable improved photocatalytic activities in comparison with ZnO nanorods. Thus, the Au nanoparticles embedded ZnO nanorods composite nanostructure improve the separation of photogenerated electron-hole pairs due to the potential energy differences between Au and ZnO, thus enhancing the photocatalytic activity.

Chapter - 5

Conclusion

Chapter - 5

Conclusion:

In summary, a novel chemical approach for the one-pot synthesis of Au nanoparticles embedded ZnO nanorods composite nanostructure and its formation chemistry have been discussed. Au nanoparticles embedded ZnO nanorods composite nanostructure caused the material to exhibit significant improvement in the photocatalytic activity. The examination of photoreduction ability shows that the Au nanoparticles embedded ZnO nanorods composite structure possess higher photoreduction ability than the bare ZnO nanorods for the degradation of MB under UV-light irradiation due to the enhanced separation efficiency of photogenerated electron-hole pairs and exhibited excellent stability (about 5% loss after 11^{th} cycles). This is not only because of the low internal resistance but also due to electrons tapping and accumulation between Au nanoparticles and ZnO nanorods interfacial Schottky barrier.(Wood et al. 2001) (Zheng et al. 2015) The design of new optical-based materials based on metal-semiconductor heterostructures has opened up new possibilities for photocatalytic and optoelectronic applications. Although many issues are to be addressed, the general interest in metal-semiconductor heterostructures is expected to grow in coming years because applications are still in the embryonic stage.

REFERENCES

REFERENCES

Barnes, W. L.Dereux, A. and Ebbesen, T. W. (2003). Surface plasmon subwavelength optics. Nature, **424**, 824.

Bera, S.Dhara, S.Velmurugan, S. and Tyagi, A. K. (2012). Analysis on binding energy and Auger parameter for estimating size and stoichiometry of ZnO nanorods. International Journal of Spectroscopy, 371092, 371094 pp.

Biesinger, M. C.Lau, L. W. M.Gerson, A. R. and Smart, R. S. C. (2010). Resolving surface chemical states in XPS analysis of first row transition metals, oxides and hydroxides: Sc, Ti, V, Cu and Zn. Applied Surface Science, **257**, 887-898.

Brongersma, M. L. and Shalaev, V. M. (2010). The case for plasmonics. Science, **328**, 440-441.

Comotti, M.Li, W.-C.Spliethoff, B. and Schueth, F. (2006). Support Effect in High Activity Gold Catalysts for CO Oxidation. Journal of the American Chemical Society, **128**, 917-924.

Dong, X.Ji, X.Wu, H.Zhao, L.Li, J. and Yang, W. (2009). Shape control of silver nanoparticles by stepwise citrate reduction. The Journal of Physical Chemistry C, **113**, 6573-6576.

Gramotnev, D. K. and Bozhevolnyi, S. I. (2010). Plasmonics beyond the diffraction limit. Nature Photonics, **4**, 83.

Haldar, K. K.Muley, V. Y.Datar, S. and Patra, A. (2017). Structural and electronic investigation of metal-semiconductor hybrid tetrapod hetero-structures. Gold Bulletin, **50**, 105-110.

Haldar, K. K. and Sen, T. (2016). Shell thickness matters! Energy transfer and rectification study of Au/ZnO core/shell nanoparticles. Advances in Colloid and Interface Science, **484**, 263-269.

Haldar, K. K.Sen, T. and Patra, A. (2008). Au@ZnO Core-Shell Nanoparticles Are Efficient Energy Acceptors with Organic Dye Donors. Journal of Physical Chemistry C, **112**, 11650-11656.

Hirakawa, T. and Kamat, P. V. (2005). Charge Separation and Catalytic Activity of Ag@TiO_2 Core-Shell Composite Clusters under UV-Irradiation. Journal of the American Chemical Society, **127**, 3928-3934.

Islam, M. N.Ghosh, T. B.Chopra, K. L. and Acharya, H. N. (1996). XPS and X-ray diffraction studies of aluminum-doped zinc oxide transparent conducting films. Thin Solid Films, **280**, 20-25.

Jiang, J.Bosnick, K.Maillard, M. and Brus, L. (2003). Single molecule Raman spectroscopy at the junctions of large Ag nanocrystals: ACS Publications.

Kamat, P. V. (2002). Photophysical, photochemical and photocatalytic aspects of metal nanoparticles: ACS Publications.

Kawata, S. (2001). Near-field microscope probes utilizing surface plasmon polaritons Near-Field Optics and Surface Plasmon Polaritons (pp. 15-27): Springer.

Kimling, J.Maier, M.Okenve, B.Kotaidis, V.Ballot, H. and Plech, A. (2006). Turkevich Method for Gold Nanoparticle Synthesis Revisited. Journal of Physical Chemistry B, **110**, 15700-15707.

Klyushin, A. Y.Rocha, T. C.Hävecker, M.Knop-Gericke, A. and Schlögl, R. (2014). A near ambient pressure XPS study of Au oxidation. Chemical physics, **16**, 7881-7886.

Kühn, S.Håkanson, U.Rogobete, L. and Sandoghdar, V. (2006). Enhancement of single-molecule fluorescence using a gold nanoparticle as an optical nanoantenna. Physical Review Letters, **97**, 017402.

Lakowicz, J. R. (2005). Radiative decay engineering 5: metal-enhanced fluorescence and plasmon emission. Analytical Biochemistry, **337**, 171-194.

Li, X.Zhang, Y. and Ren, X. (2009). Effects of localized surface plasmons on the photoluminescence properties of Au-coated ZnO films. Optics Express, **17**, 8735-8740.

Liang, J.Peng, Q.Wang, X.Zheng, X.Wang, R. (2005). Chromate nanorods/nanobelts: general synthesis, characterization, and properties. Inorganic chemistry, **44**, 9405-9415.

Link, S. and El-Sayed, M. A. (1999). Size and temperature dependence of the plasmon absorption of colloidal gold nanoparticles. The Journal of Physical Chemistry B, **103**, 4212-4217.

Liu, B. and Zeng, H. C. (2003). Hydrothermal Synthesis of ZnO Nanorods in the Diameter Regime of 50 nm. Journal of the American Chemical Society, **125**, 4430-4431.

Mar, L. G.Timbrell, P. Y. and Lamb, R. N. (1993). An XPS study of zinc oxide thin film growth on copper using zinc acetate as a precursor. Thin Solid Films, **223**, 341-347.

Nie, S. and Emory, S. R. (1997). Probing single molecules and single nanoparticles by surface-enhanced Raman scattering. Science, **275**, 1102-1106.

Oldfield, G.Ung, T. and Mulvaney, P. (2000). Au@SnO_2 Core-Shell nanocapacitors. Advanced Materials, (Weinheim, Ger.), **12**, 1519-1522.

Rang, M.Jones, A. C.Zhou, F.Li, Z.-Y.Wiley, B. J. (2008). Optical near-field mapping of plasmonic nanoprisms. Nano Letters, **8**, 3357-3363.

Rao, C.Kulkarni, G.Thomas, P. J. and Edwards, P. P. (2002). Size-dependent chemistry: properties of nanocrystals. Chemistry-A European Journal, **8**, 28-35.

Ruiz Peralta, M. D. L.Pal, U. and Zeferino, R. S. (2012). Photoluminescence (PL) Quenching and Enhanced Photocatalytic Activity of Au-Decorated ZnO Nanorods Fabricated through Microwave-Assisted Chemical Synthesis. ACS Applied Materials & Interfaces **4**, 4807-4816.

She, P.Xu, K.Shang, Y.He, Q.Zeng, S. (2018). ZnO nanodisks decorated with Au nanorods for enhanced photocurrent generation and photocatalytic activity. New Journal of Chemistry, **42**, 3315-3321.

Singh, S.Ahmed, I. and Haldar, K. K. (2018). Nickel oxide decorated zinc oxide composite nanorods: Excellent catalyst for photoreduction of hexavalent chromium. Journal of colloid and interface science, **523**, 1-6.

Soltani, N.Saion, E.Hussein, M. Z.Erfani, M.Abedini, A. (2012). Visible light-induced degradation of methylene blue in the presence of photocatalytic ZnS and CdS nanoparticles. International Journal of Molecular Sciences, **13**, 12242-12258.

Stockman, M. I. (2011). Nanoplasmonics: The physics behind the applications. Physics Today, **64**, 39-44.

Strunk, J.Kaehler, K.Xia, X.Comotti, M.Schueth, F. (2009). Au/ZnO as catalyst for methanol synthesis: The role of oxygen vacancies. Applied Catalysis A, **359**, 121-128.

Sun, Y.Gates, B.Mayers, B. and Xia, Y. (2002). Crystalline silver nanowires by soft solution processing. Nano Letters, **2**, 165-168.

Tahir, M. N.Natalio, F.Cambaz, M. A.Panthoefer, M.Branscheid, R. (2013). Controlled synthesis of linear and branched Au@ZnO hybrid nanocrystals and their photocatalytic properties. Nanoscale, **5**, 9944-9949.

Wang, Y.Zhang, Z.Zhu, Y.Li, Z.Vajtai, R. (2008). Nanostructured VO_2 photocatalysts for hydrogen production. Acs Nano, **2**, 1492-1496.

Wiley, B.Sun, Y. and Xia, Y. (2007). Synthesis of silver nanostructures with controlled shapes and properties. Accounts of Chemical Research, **40**, 1067-1076.

Wood, A.Giersig, M. and Mulvaney, P. (2001). Fermi level equilibration in quantum dot-metal nanojunctions. Journal of Physical Chemistry B, **105**, 8810-8815.

Wu, C.-H. and Chern, J.-M. (2006). Kinetics of photocatalytic decomposition of methylene blue. Industrial & Engineering Chemistry Research, **45**, 6450-6457.

Yang, Y. W. and Fan, L. J. (2002). High-Resolution XPS Study of Decanethiol on Au(111): Single Sulfur-Gold Bonding Interaction. Langmuir, **18**, 1157-1164.

Yu, Y.-Y.Chang, S.-S.Lee, C.-L. and Wang, C. C. (1997). Gold nanorods: electrochemical synthesis and optical properties. The Journal of Physical Chemistry B, **101**, 6661-6664.

Zheng, X.Yan, X.Sun, Y.Bai, Z.Zhang, G. (2015). Au-Embedded ZnO/NiO Hybrid with Excellent Electrochemical Performance as Advanced Electrode Materials for Supercapacitor. ACS Applied Materials & Interfaces, **7**, 2480-2485.